

# Seismic rehabilitation of substandard RC columns with partially deteriorated concrete using CFRP composites

Dongxu Hou<sup>1</sup>, Zhimin Wu<sup>\*1</sup>, Jianjun Zheng<sup>2</sup> and Yao Cui<sup>1c</sup>

<sup>1</sup>State Key Laboratory of Coastal and Offshore Engineering, Dalian University of Technology,  
No.2 Linggong Road, Ganjingzi District, Dalian City, The Peoples' Republic of China

<sup>2</sup>School of Civil Engineering and Architecture, Zhejiang University of Technology,  
No.18 Chaowang Road, Xiacheng District, Hangzhou City, The Peoples' Republic of China

(Received November 4, 2013, Revised September 8, 2014, Accepted November 3, 2014)

**Abstract.** Many existing reinforced concrete (RC) columns in structures tend to become substandard RC ones due to updated standards or environmental changes. These substandard columns may alter the behaviors of the whole structure and therefore are in urgent need of seismic retrofitting. Owing to their superior advantages, carbon fiber reinforced polymer (CFRP) composites are widely used to retrofit RC columns. The applications mainly focus on various substandard RC columns, but few deals with substandard columns with deteriorated concrete, especially damaged by earthquake. The purpose of this paper is to investigate the seismic behaviors of CFRP reinforced partially deteriorated RC columns and to evaluate the effect of CFRP sheets on them. Six flexure-dominant columns were tested under a constant axial load and transverse cyclic displacements. It is found that the seismic behaviors of partially deteriorated columns can be recovered by wrapping CFRP sheets on them. Numerical analysis is then conducted using finite element methods and verified with experimental results. The effects of the axial load ratio, the ratio of the thickness of CFRP sheet to the column diameter, and the slenderness ratio on the seismic behaviors of CFRP reinforced RC columns are evaluated. Finally, a method is proposed to determine the required thickness of CFRP sheet.

**Keywords:** substandard RC column; partially deteriorated concrete; seismic behavior; CFRP sheet

## 1. Introduction

Substandard RC columns are ones with inferior performance by current standards. Many factors, including environmental corrosion, freezing, and thawing, may cause RC columns to partially deteriorate, alter the original behaviors, and become a potential hazard during earthquake. Therefore, it is necessary to take effective measures to upgrade the seismic behaviors of substandard RC columns with partially deteriorated concrete.

Besides some traditional methods to strengthen RC structures, such as Yu *et al.* (2014), carbon fiber reinforced polymer (CFRP) composites have been widely used to retrofit RC members in the past decades due to their advantages. Wrapping CFRP sheets is an effective method to improve the seismic performance of RC columns (Frangou *et al.* (1995), Pantelides *et al.* (1999), and Manuel

---

\*Corresponding author, Professor, E-mail: wuzhimin@dlut.edu.cn

and Silva (2011)). Saadatmanesh *et al.* (1997a), Saadatmanesh *et al.* (1997b), Saadatmanesh *et al.* (1994), and Saadatmanesh *et al.* (1996) mainly focused on the ductility and strength of circular bridge piers retrofitted with fiber composites under earthquake and concluded that the seismic resistance of retrofitted columns can be improved significantly. Xiao *et al.* (1999) studied the shear strength of RC columns wrapped with prefabricated composite jacketing. Test results showed that both the shear strength and the ductility of columns increase remarkably. Seible *et al.* (1997) developed a new seismic retrofit system for RC columns with continuous carbon fiber jackets, which showed that the retrofitting criteria of steel jackets are applicable to carbon fiber jackets. Sheikh and Bayrak (2001), Sheikh and Yau (2002), and Iacobucci *et al.* (2003) examined the seismic behaviors of retrofitted rectangular and circular columns. The results showed that the CFRP retrofitting effect depends on the compressive strength of concrete, the thickness of CFRP sheet, and the arrangement of steel bars.

The seismic behaviors of substandard RC columns wrapped with CFRP composites were also investigated. Since RC columns are sensitive to environmental changes, more and more researchers have attempted to restore the seismic behaviors of substandard columns with CFRP composites. For example, Haroun and Elsanadedy (2005), ElGawady *et al.* (2010), and Harajli (2008) studied the seismic retrofitting of substandard columns with insufficient lap-splice lengths with CFRP sheets. Pantazopoulou *et al.* (2001) and Li *et al.* (2009) studied the CFRP upgrading of the seismic behaviors of substandard RC columns with corroded reinforcement, which is common for old RC columns. Bailey and Yaqub (2012) recovered the ductility and strength of substandard RC columns suffered from fire disaster with CFRP sheets, but the stiffness was seldom affected. Li *et al.* (2003) proposed a fast curing method to recover the compressive strength of pre-damaged RC columns. The pre-damage was realized by compressing specimens up to cracking. It was found that the bearing capacity of pre-damaged specimens recover to the undamaged level after retrofitted with GFRP. Bao and Li (2010) studied the compressive strength degradation of pre-damaged RC columns subjected to simulated impact and concluded that the residual strength of pre-damaged specimens increases with the increment of the reinforcement ratio but decreases with an increase in the aspect ratio. Li and Lim (2010) mainly focused on the seismic rehabilitation of RC walls with FRP and demonstrated that damaged RC walls repaired with FRP are able to restore the performance effectively. Thermou and Pantazopoulou (2009) studied the seismic rehabilitation of FRP by previously damaged RC columns and found that the undesired failure mode of pre-damaged columns can be altered by FRP jacketing. Saadatmanesh *et al.* (1997a) demonstrated that wrapping CFRP sheets is effective in improving the flexural strength and ductility of flexure-dominant RC columns. Fukuyama *et al.* (2000) examined the recoverability of lateral bearing capacity and the ductility of CFRP repaired RC columns and indicated that the lateral bearing capacity and ductility of damage columns can be restored to the undamage level.

Deteriorated substandard RC columns due to concrete quality have also been investigated. Many factors may deteriorate intact concrete members, especially existing old concrete structures. Lower strength is possibly the most important factor (Hanjari (2010), Emmanuel and Oladipo (2012), and Belarbi and Bae (2007)). Manuel and Silva (2011), Rousakis and Karabinis (2008) and Akgun *et al.* (2010) used concrete with compressive strengths of 9.7 MPa and 12.5 MPa to simulate existing old concrete structures and examined the axial compressive behavior of substandard columns. Yalcin and Kaya (2004) and Yalcin *et al.* (2008) cast RC columns with a compressive strength of 15 MPa to simulate poor concrete caused by construction quality, and found that the lateral bearing capacity and ductility of CFRP retrofitted low strength RC columns increase significantly. Ozcan *et al.* (2008) and Ozcan *et al.* (2010) mainly focused on the seismic

rehabilitation of common columns in an old structure of Turkey and simulated the strength degradation of concrete, and found that increasing the confinement ratio enables the CFRP retrofitted column to sustain a higher ultimate drift capacity. Goksu *et al.* (2012) intentionally used concrete with a compressive strength of 9.3 MPa and plain bars to model relatively old, existing substandard columns, and indicated that the new retrofitted technology using CFRP sheets and anchorage is effective in avoiding the buckling or shear damage of columns and the debonding of CFRP. Pantazopoulou *et al.* (2001) that the performance is markedly improved when increasing the number of FRP layers. Kalyoncuoglu *et al.* (2013) studied the seismic behaviors of substandard columns by using concrete with a compressive strength of 4 MPa and showed that the lower strength may lead to the bearing capacity degradation and increase of deformations.

As mentioned above, many researchers have paid attention to deteriorated concrete in structures, and low-strength concrete was adopted to simulate deteriorated concrete widely. There are limited studies available in the literature on substandard RC columns with partially deteriorated concrete. Wei *et al.* (2009), Wei *et al.* (2010), and Wei (2009) have performed experiments aimed at the recoverability of CFRP confined partially deteriorated RC columns under axial and eccentric loads. The results indicated that the load bearing capacity can be recovered with sufficient amount of CFRP sheets. Although many researchers have used concrete with reduced strength to investigate the behaviors of substandard concrete members, the limitation of this method need to be clarified. This concrete is equivalent to deteriorated concrete only in strength. Therefore, this simplification is suitable for studying the adverse influence of deteriorated concrete on the behaviors of concrete members.

As an extension of Wei *et al.*'s studies, this paper aims to investigate the seismic performance of substandard RC columns with partially deteriorated concrete and to evaluate the recoverability using CFRP sheets. Six flexure-dominant RC columns were tested under a constant axial load and transverse cyclic loads. A nonlinear finite element method is conducted to evaluate the effects of various factors on the seismic behaviors of partially deteriorated RC columns. Finally, a method is proposed to determine the required thickness of CFRP sheets.

## 2. Experimental program

### 2.1. Specimens

A total of six specimens, one control column and five partially deteriorated RC columns, were tested in the experiment. The design strength of concrete was 50 MPa for the control column, and 30 MPa and 40 MPa for simulating the partially deteriorated concrete. The initial and substandard strengths of concrete are denoted by  $f_{in}$  and  $f_w$ , respectively. The cantilever circular columns had a length  $L$  of 1300 mm and a diameter  $D$  of 240 mm and were reinforced with six longitudinal deformed steel bars with a diameter of 16 mm. The cover depth was 25 mm. The volumetric ratios of longitudinal and transverse bars were 2.66% and 1.2%, respectively. The stirrups were composed of plain bars with a diameter of 8 mm and a spacing of 100 mm.

A deteriorated portion with a length of 250 mm was artificially made at the column foot, as shown in Fig. 1. The stub was cast firstly, and the deterioration and intact portions of the column were then cast using two types of concrete designed above, respectively. There are no construction joints between the deterioration and intact portions. Substandard RC columns were wrapped with CFRP sheets with different thicknesses  $t$ . The details of the specimens are listed in Table 1.

Table 1 Details of specimens

Specimen	$f_w$ (MPa)	$t$ (mm)
DB50	-	-
BR200	22	0
BR300	31	0
BR301	31	0.167 (1 layer)
BR302	31	0.334 (2 layers)
BR203	22	0.501 (3 layers)

## 2.2. Material properties

Commercial ready-mixed concrete with a compressive strength of 52 MPa was used as intact concrete, while two types of concrete, C1 and C2, were prepared for partially deteriorated concrete. C1 and C2 were made with two different mix proportions and silicate cements with standard 28-day compressive strengths of 32.5 and 42.5 MPa and the measured compressive strengths were 31 and 22 MPa, respectively. Crushed limestone with a maximum size of 20 mm was used as coarse aggregate and river sand as fine aggregate. The mix proportions and properties of concrete are shown in Table 2. The material properties of steel bars and CFRP sheets are listed in Tables 3 -4, respectively. The yield strength  $f_y$ , ultimate strength  $f_u$ , and elastic modulus  $E_s$  of steel bars and the tensile strength  $f_{cfpr}$  and elastic modulus  $E_{cfpr}$  of CFRP were determined from the coupon test.

## 2.3 Test instrumentation

As shown in Fig. 2(a), two displacement transducers were placed at the top of the column and the other two at the upper end of the deteriorated segment to record the horizontal displacements. They were installed on two steel angles fixed on the footing of the specimen to measure the relative displacement between the column and the stub. All the instrumentations were connected to an IMC data acquisition system and a microcomputer for data collecting. The arrangement of strain gauges is shown in Fig. 1. Strain gauges (SG1) of 1 mm  $\times$  2 mm were bonded on each steel bar with an interval of 100 mm to monitor the yielding of longitudinal bars. Two groups of vertical and horizontal strain gauges were located at the two sides of the column section to monitor the vertical and horizontal strains of the plastic hinge region during loading. Strain gauges (SG2) of 20 mm  $\times$  2 mm and strain gauges (SG3) of 80 mm  $\times$  2 mm were bonded on the CFRP retrofitted and un-retrofitted columns, respectively.

The specimen was placed within an existing testing frame, as shown in Fig. 2(b). The column stubs with a width of 1300 mm were compacted by two steel beams, which were fastened to the rigid floor with four high-strength rods, to prevent slipping and overturning since the width of the rods channel was 1100 mm. The stubs of the specimen were also fastened by two transverse jacks to eliminate transverse movements during loading. A hydraulic actuator with a load cell of 2000 kN was mounted vertically onto the frame to apply the axial load and other two with a load cell of 300 kN were used to apply lateral loads. Two jacks were installed at the two sides of the column footing to prevent it from moving during loading.

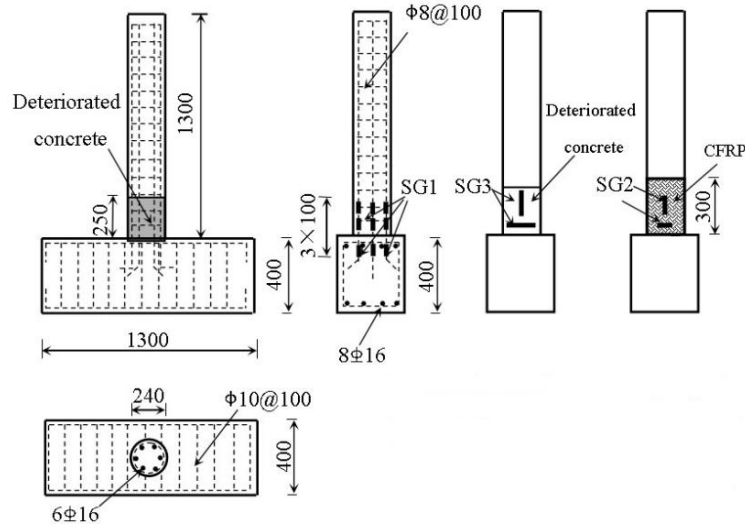


Fig. 1 Details of RC specimen (mm)

Table 2 Mix proportions of concrete ( $\text{kg}/\text{m}^3$ )

Concrete type	Coarse aggregate	Fine aggregate	Cement	Water
Ready-mix	1400	927	591	195
C1	1134	638	433	195
C2	1121	630	453	195

Table 3 Properties of steel bars

Bar type	$f_y$ (MPa)	$f_u$ (MPa)	$E_s$ (GPa)
Deformed bar	360	580	206
Plain bar	290	420	210

Table 4 Properties of CFRP composites

Type	$f_{cfpr}$ (MPa)	$E_{cfpr}$ (GPa)
CFRP sheet	3400	235
Epoxy resin	40	2.5

All the columns were tested under a constant axial load and transverse cyclic loads. The axial load  $P$  was maintained on the top of the column at  $0.1f_{in}A$ , i.e., 200 kN, where  $A$  is the cross sectional area of the column. Under a sustained constant axial load, horizontal loading was applied in a load-controlled and displacement-controlled manner before and after the stress in longitudinal bars reached the yield strength, respectively, as shown in Fig. 3, where  $\delta$  is the displacement at the top of the column and  $\delta_y$  is the yield displacement. When the bending moment of the concrete column reaches 85% of the ultimate bearing capacity, it is said that the column fails.

## 2.4. Experimental results

### 2.4.1 Test observations

When testing control column DB50, it was observed that the first transverse crack occurred in the tension zone when the lateral displacement was about 0.4% drift. The position of the first crack was about 60 mm above the base. When the lateral displacement was 1% drift, the lateral resistance reached its peak value. With the increase of the lateral load, more transverse flexural cracks appeared along the column up to 1000 mm above the base with a space of about 100 mm, as shown in Figs. 4(a)-(d). This can be explained as follows. When the column is subjected to a small axial load, the height of the compression zone of the column is small and the bending moment is resisted by the longitudinal bars and concrete in the tension zone. Since the ultimate tensile strain of concrete is much smaller than that of steel bars, more and more transverse cracks occurred during loading. When the lateral displacement was about 1.4% drift, two vertical cracks appeared in the compression zone of the specimen. The concrete in the compression zone began to crush. The control column failed at a lateral displacement of 3.3% drift, with longer vertical cracks and significant spalling of the concrete cover, as shown in Fig. 4(g).

On partially deteriorated columns BR200 and BR300, the first and second transverse cracks appeared in the tension zone when the lateral displacement was 0.35% drift and 0.4% drift, respectively. The locations of the transverse cracks are about 60 mm and 110 mm above the base. Different from control column DB50, no more transverse cracks were observed along the height of the column. When the lateral displacement was about 0.8% drift and 1.0% drift, the lateral resistance of BR200 and BR300 reached their peak values, respectively, and several vertical cracks appeared in the compression zone. With the increase of the lateral load, the transverse and vertical cracks propagated rapidly and linked together. The partially deteriorated columns failed at a lateral displacement of about 2.9% drift. The deteriorated segment was severely damaged as shown in Fig. 4(b) and 4(e).

Compared with partially deteriorated columns BR200 and BR300, CFRP retrofitted substandard columns BR301, BR302, and BR203 exhibited excellent seismic behaviors. Noise was clearly heard after 1.0% drift, when the epoxy between the CFRP jacket and column cracked. The lateral resistances reached their peak values when the lateral displacements were 1.8% drift, 2.0% drift, and 1.7% drifts, respectively. When the lateral displacements were 3.2% drift, 4.0% drift, and 4.3% drift, respectively, the wrapped CFRP sheets swelled seriously with brittle sound. The tests were stopped at lateral displacements of 4.3% drift, 4.9% drift, and 5.3% drift, respectively. Few CFRP fibers at the foot of the column were ruptured, and many transverse cracks appeared along the height above the CFRP-wrapped zone, as shown in Fig. 4(c), 4(f), and 4(h). It should be pointed out that no obvious inclined cracks appeared on specimens, as shown in Figs. 4(a)-(h). This can be explained as follows. For each specimen, the axial load ratio is smaller than 0.3, while the slenderness ratio is larger than 5, which indicates that the specimens are flexure-dominant. Therefore, inclined cracks do not occur during loading.

### 2.4.2 Hysteretic loops and envelope curves

The hysteretic loops of specimens are shown in Figs. 5(a)-(f). The lateral bearing capacity and the drift ratio at the peak bearing capacity for the pushing cycle in the positive direction seems slightly higher than those for the pulling cycle in the negative direction. The difference of bearing capacity between them is caused by the Bauschinger effect of longitudinal steel bars.

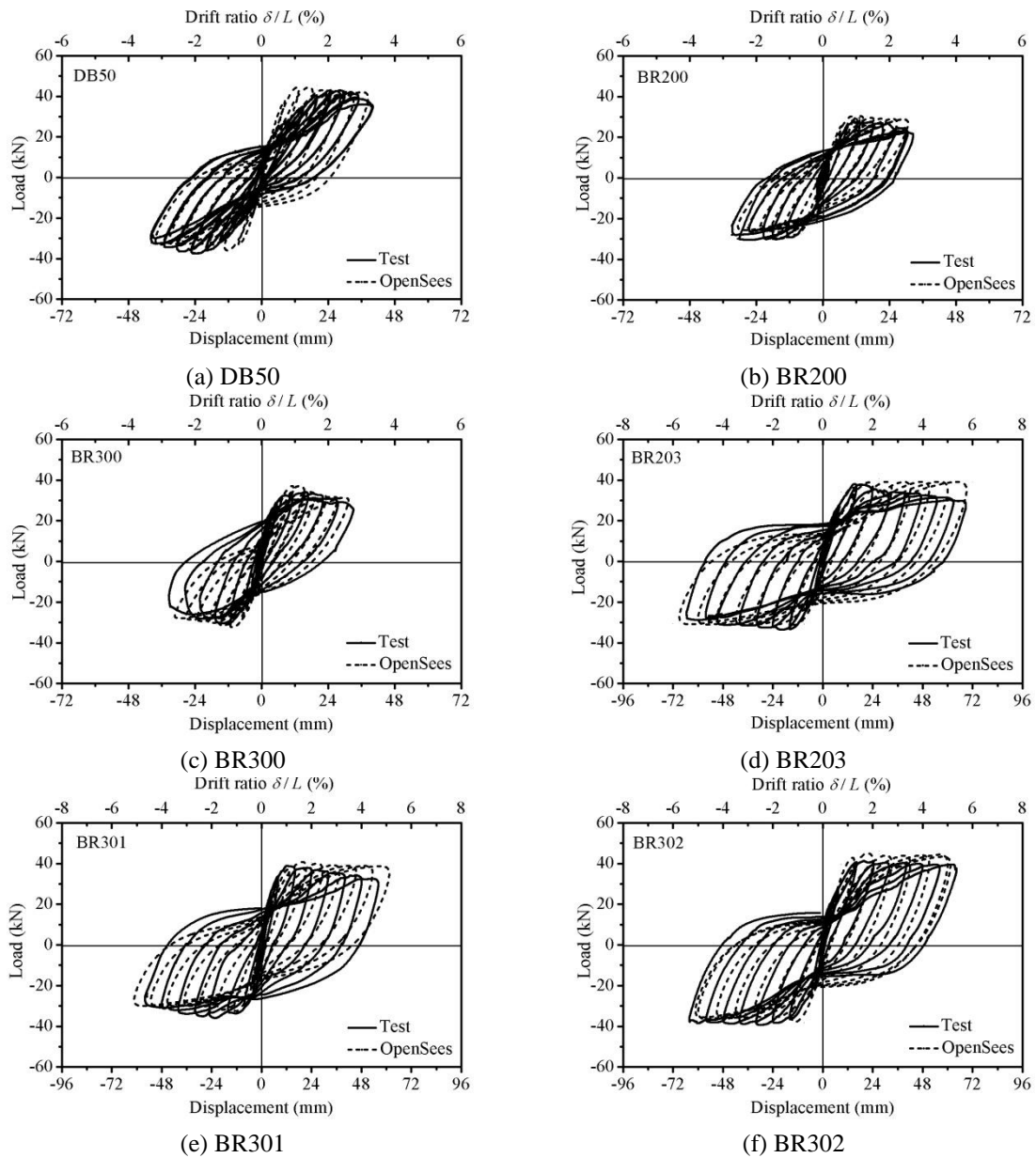


Fig. 5 Comparison of hysteretic loop between experimental results and numerical results

The envelope curves of columns are shown in Figs. 6(a)-(d). As can be seen from Fig. 6(a), although the deterioration of columns is local, the seismic behavior is greatly reduced. The lateral bearing capacities  $P_{exp}$  of partially deteriorated columns BR300 and BR200 are 35.6 kN and 29.8 kN, respectively. Compared with the 42.6 kN lateral bearing capacity of intact column DB50, their lateral bearing capacities decrease by 17% and 30%, respectively. The ultimate drift ratios of BR200, BR300, and DB50 are 2.8%, 2.9%, and 3.3%, respectively. In this paper, the ultimate

lateral displacement is equal to that of columns at failure and the ultimate drift ratio is defined as the ratio of the ultimate lateral displacement to the length of columns. The significant reduction of ultimate drift ratios for BR200 and BR300 is mainly due to the larger axial load ratios of partially deteriorated columns compared with that of specimen DB50.

It is showed that partially deteriorated concrete has more remarkable influence on the lateral bearing capacity than the drift ratio. Figs. 6(b)-(c) are the comparison of the envelope curves of partially deteriorated and retrofitted columns. Fig. 6(b) shows that the lateral bearing capacity of retrofitted column BR203 is 39.1 kN. After retrofitting three layers of CFRP sheets, the lateral bearing capacity increases by 31%. The ultimate drift ratio of retrofitted column BR203 is 5.3%, 1.8 times that of substandard column BR200. In Fig. 6(c), the lateral bearing capacities of substandard columns increase by 9.2% and 15% when one layer and two layers of CFRP sheets were adopted, respectively. The ultimate drift ratios increase by 58.6% and 82.7% compared with that of BR300. The envelope curves of CFRP retrofitted columns and intact column DB50 were compared in Fig. 6(d), which indicates that the difference in lateral bearing capacity between retrofitted columns and intact column is smaller than 10%, whereas the drift ratios of retrofitted columns are at least 1.5 times that of the intact column. It can be concluded that, by retrofitting CFRP sheets, the seismic behaviors of partially deteriorated columns can be recovered.

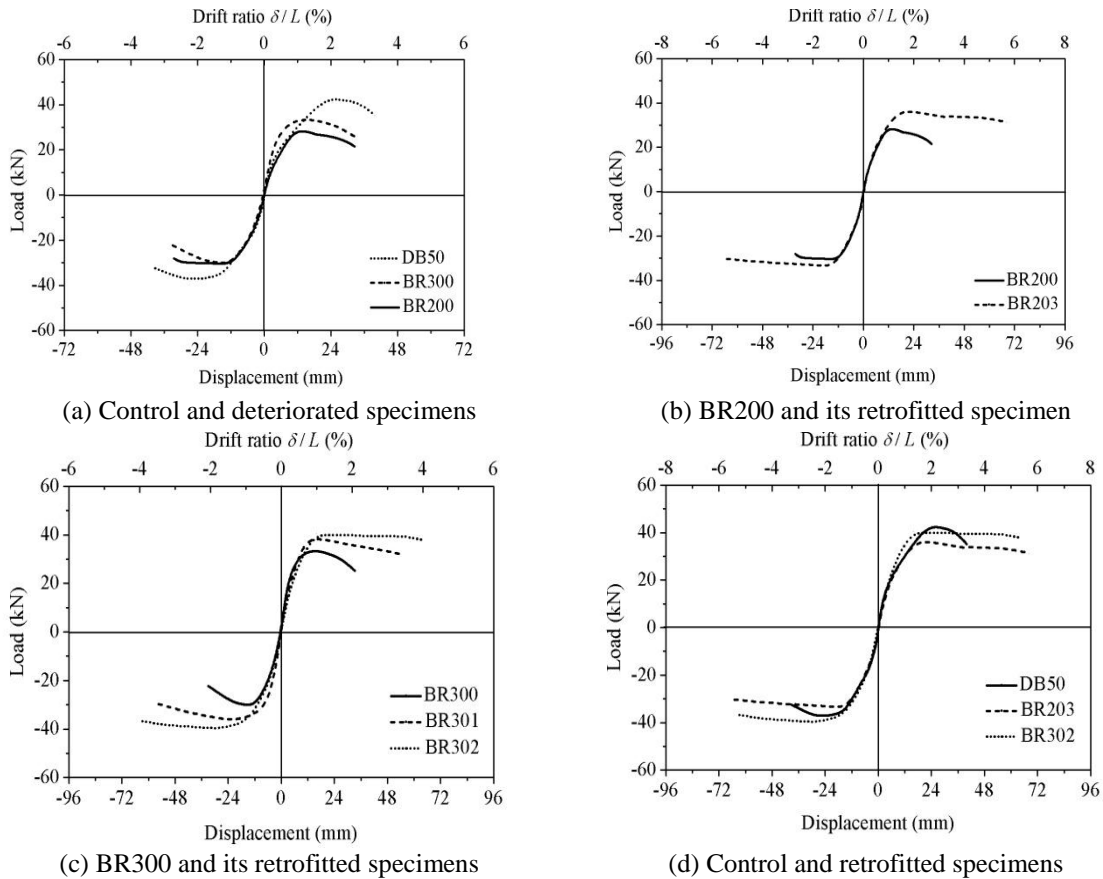


Fig. 6 Envelope curves of specimens

Table 5 Test results

Specimen	$P_{exp}$ (kN)	$\delta_y$ (mm)	$\mu$	$k_0$ (kN/mm )	$E_d$ (kN·m)
DB50	42.6	6.9	5.8	6.4	17.9
BR200	29.8	7.6	4.2	5.2	22.4
BR300	35.6	7.2	4.8	6.1	18.4
BR301	38.9	8.6	6.5	6.5	40.7
BR302	41.0	8.7	7.4	6.6	54.2
BR203	39.1	8.7	8.3	7.0	69.8

### 2.4.3 Strains in longitudinal bars

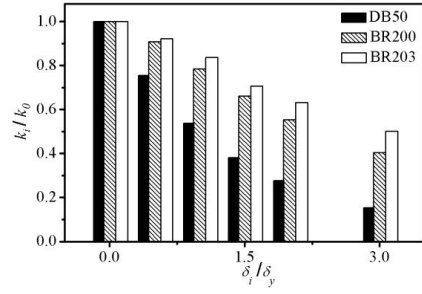
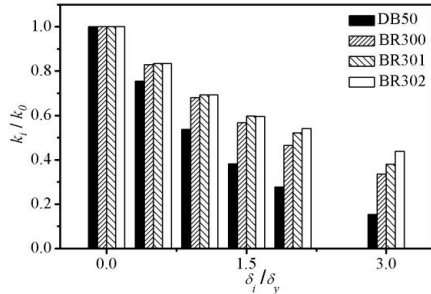
The arrangement of strain gauges along longitudinal bars is shown in Fig. 1. The strain in each steel bar in the plastic hinge zone was recorded by three strain gauges. Fig. 7 shows the tensile strains at SG1 and SG2 during loading. According to the properties of steel bars shown in Table 3, the yield strain is taken as 0.0017. When the strain at SG1 or SG2 is equal to the yield strain, it is said that the column is in the yield state. As can be seen from Fig. 1, the yield drift ratios of control column DB50, and partially deteriorated columns BR200 and BR300 are 0.57%, 0.63%, and 0.60%, while those of CFRP retrofitted columns BR301, BR302, and BR203 are 0.72%, 0.73%, and 0.73%, respectively, which indicates that wrapping CFRP sheets is effective in delaying the yielding of steel bars.

### 2.4.4 Ductility index analysis

The ductility of RC columns is represented by the ductility index  $\mu$ , which is the ratio of the ultimate displacement  $\delta_u$  to the yield displacement  $\delta_y$ . The ductility index  $\mu$  and  $\delta_y$  of specimens are shown in Table 5. It can be seen from Table 5 that the ductility index of control column DB50 is 5.8, while those of partially deteriorated columns BR200 and BR300 are 4.2 and 4.8, respectively, which indicates that the ductility of RC columns is decreased by partially deteriorated concrete. Although deteriorated concrete is replaced with concrete with reduced strength, specimens are subjected to the same axial load but different axial load ratios. The axial load ratios of specimens BR200 and BR300 are much larger than that of control specimen DB50. Therefore, the ductility of partially deteriorated specimens is lower than that of the intact specimen. Compared with partially deteriorated columns, the ductility indexes of retrofitted columns BR301, BR302, and BR203 are 6.5, 7.4, and 8.3, respectively. Therefore, wrapping CFRP sheets is effective in recovering the ductility of columns.

### 2.4.5 Stiffness degradation

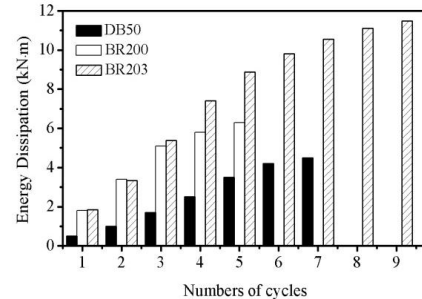
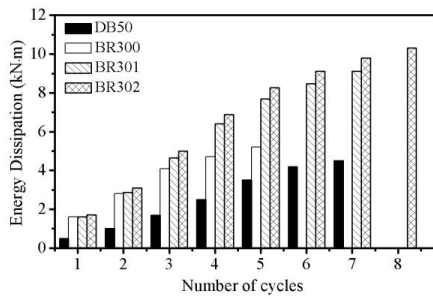
Figs. 8(a)-(b) show the stiffness degradation ratio  $k_i/k_0$ , where  $k_0$  is the initial stiffness, and  $k_i$  and  $\delta_i$  are the stiffness and displacement at the  $i^{\text{th}}$  hysteretic loop, respectively. It can be seen from Figs. 8(a)-(b) that, when the displacement is smaller than 1.5 times the yield displacement, the difference in stiffness degradation ratio between substandard and retrofitted columns is smaller than 1%. When the displacement is larger than 1.5 times the yield displacement, however, retrofitted columns exhibit larger stiffness.



(a) DB50, BR300 and retrofitted specimens

(b) DB50, BR200 and retrofitted specimen

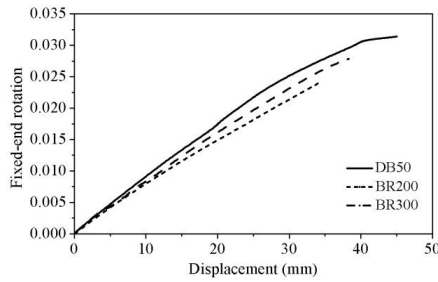
Fig. 8 Stiffness degradations of substandard and retrofitted columns



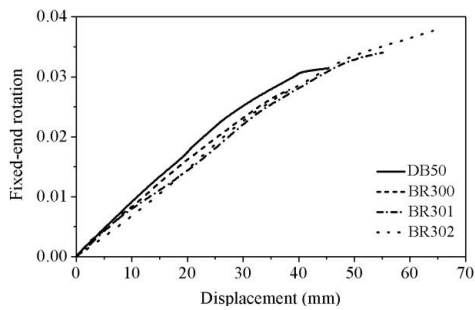
(a) DB50, BR300 and retrofitted specimens

(b) DB50, BR200 and retrofitted specimen

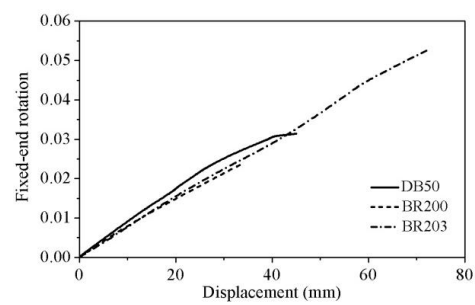
Fig. 9 Energy dissipations of specimens at different cycles



(a) Control and deteriorated specimens



(b) DB50, BR300 and retrofitted specimens



(c) DB50, BR200 and retrofitted specimen

Fig. 10 Relationships between fixed-end rotation and displacement of specimens

### 2.4.6 Energy dissipation

The energy dissipation  $E_d$  of a specimen is defined as the area under the hysteretic loop curve. The energy dissipations of specimens are shown in Table 5. It can be seen from Table 5 that wrapping one layer, two layers, and three layers of CFRP sheets can increase the energy dissipation by 1.2, 1.9, and 2.1 for substandard RC columns.

The energy dissipation capacities at all cycles are shown in Figs. 9(a)-(b), which indicates that the incremental energy dissipation becomes smaller by increasing the number of cycles for the three types of specimens and that the energy dissipation of partially deteriorated columns is seldom affected by CFRP sheets for the first three cycles.

### 2.4.7 Fixed-end rotation

The horizontal displacements of deteriorated concrete segments were measured by the two displacement transducers shown in Fig. 2(a). The comparisons of the fixed-end rotation to the lateral displacement at the column top are shown in Figs. 10(a)-(c). It can be seen from Fig. 10(a) that the fixed-end rotations of specimens are almost same at the beginning of test. With the increase of the lateral displacement, the fixed-end rotations of partially deteriorated specimens become smaller due to the smaller stiffness of the deteriorated concrete segment. Figs. 10(b)-(c) show that the fixed-end rotations of deteriorated and retrofitted columns are almost the same. This indicates that CFRP sheets cannot improve the stiffness of the deteriorated concrete segment.

## 3. Finite element analysis

To further study the seismic behaviors of partially deteriorated RC columns, a finite element analysis was conducted based on OpenSees (Mazzoni *et al.* 2009). The material properties are listed in Tables 2-4. In the analysis, the plane cross-section assumption was adopted, the interfaces between steel bars, CFRP sheets, and concrete were perfect, and the shear effect was neglected (Zhu *et al.* 2006). The confinement effects of stirrups were ignored, but the P-delta effect was considered.

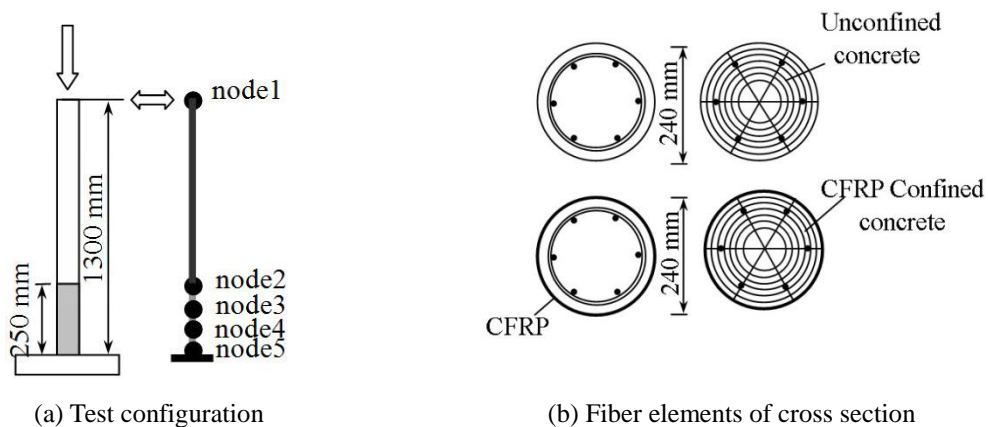


Fig. 11 Finite element analysis models

### 3.1 Geometric models

A fiber section is assigned to the beam-column elements to describe the nonlinear behaviors of partially deteriorated RC columns. Different constitutive relationships are adopted for the confined concrete, unconfined concrete and longitudinal reinforcement fibers. The column is composed of two segments: deteriorated or strengthened and intact. Nodes 1 and 5 are at the top and bottom, respectively, and node 2 separates the two segments. For partially deteriorated and retrofitted specimens, nodes 3 and 4 are used to divide the region between nodes 2 and 5. The column base is modeled as a fixed end and the axial load and transverse reversed cyclic displacement are applied at the top node, as shown in Figs. 11(a)-(b). The lateral action analysis is conducted by the displacement controlled method.

### 3.2 Constitutive models of materials

The main parameters used in the finite element analysis are listed in Table 6. As shown in Fig. 12(a), the stress-strain relationship for unconfined concrete consists of an ascending parabola OA, a descending line AB, and a residual line BC (Kent and Park (1971)), where  $\sigma_A$  and  $\varepsilon_A$  are obtained through axial compressive tests and  $\sigma_B$ ,  $\varepsilon_B$ , the tensile strength  $f_t$ , and the fracture energy  $G_f$  are estimated from CEB-FIP2010 (CEB-FIP. 2010).  $\varepsilon_0$  and  $\varepsilon_{cu}$  are the strains at the peak point and ultimate point of unconfined concrete. For CFRP confined concrete, the Teng et al. model, Teng *et al.* (2009) and Lam and Teng (2003), is adopted. The stresses and strains at points A and B are determined from this model and the tensile strength and fracture energy are taken the same as those of unconfined concrete,  $f_{cc}$  and  $\varepsilon_{cc}$  are the ultimate stress and strain of confined concrete. FRP confined concrete is simulated by projecting the stresses and strains at points A and B of FRP confined concrete onto the module Concrete02 in OpenSees. The cyclic behavior of Concrete02 is based on the results of Scott *et al.* (1982). For steel bars, the modified model of Giuffr -Menegotto-Pinto is adopted, as shown in Fig. 12(b), where  $f_y$ ,  $E_s$ ,  $E_h$  are listed in Table 6.

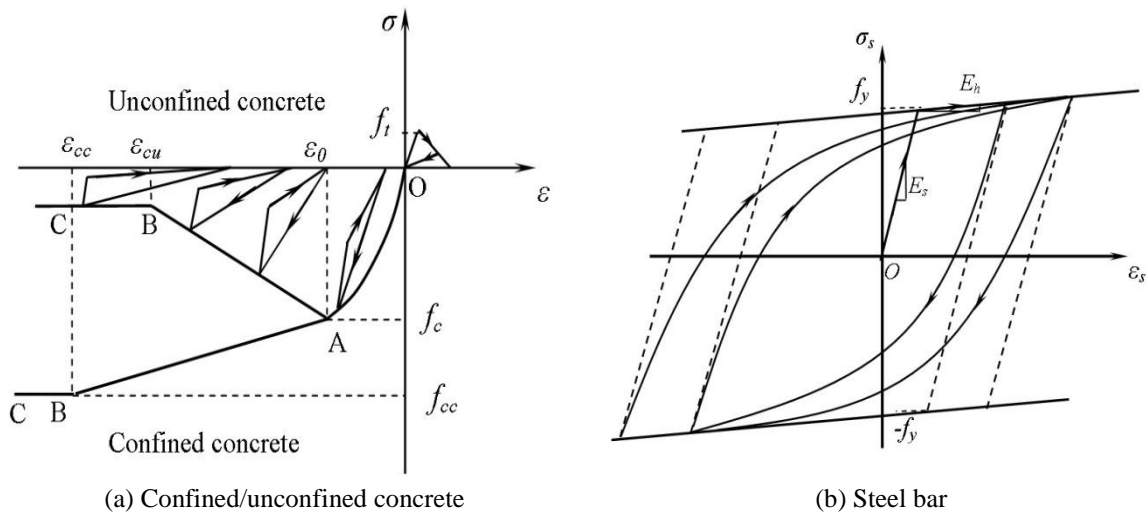


Fig. 12 Constitutive models of unconfined concrete, confined concrete, and steel bar

Table 6 Input parameters for finite element analysis

Specimen	$\sigma_A$ (MPa)	$\varepsilon_A$	$\sigma_B$ (MPa)	$\varepsilon_B$	$f_t$ (MPa)	$G_f$ (N/m)	$f_y$ (MPa)	$E_s$ (GPa)	$E_h$ (GPa)
DB50	52.0	0.0024	42.5	0.0030	4.2	152.5	360	206	2.06
BR300	31.0	0.0023	26.0	0.0033	3.0	141.1	360	206	2.06
BR301	32.9	0.0024	40.2	0.0112	3.0	141.1	360	206	2.06
BR302	33.7	0.0024	49.3	0.0166	3.0	144.7	360	206	2.06
BR200	22.0	0.0022	18.7	0.0033	2.4	134.6	360	206	2.06
BR203	23.9	0.0022	49.5	0.0287	2.4	134.6	360	206	2.06

Table 7 Comparison of bearing capacity between experimental results and numerical results

Specimen	$P_{exp}$ (kN)	$P_{sec}$ (kN)	$\frac{ P_{sec} - P_{exp} }{P_{exp}} \times 100\%$	$P_{num}$ (kN)	$\frac{ P_{num} - P_{exp} }{P_{exp}} \times 100\%$
DB50	42.6	43.2	1.4%	46.8	9.8%
BR300	35.6	36.3	2.0%	37.8	6.2%
BR301	38.9	42.5	9.2%	42.0	8.0%
BR302	41.0	42.9	4.6%	43.2	5.3%
BR200	29.8	33.3	11.7%	32.4	8.7%
BR203	39.1	42.6	9.0%	41.6	6.4%

### 3.3 Model verification

With these models and input parameters, the numerical results are compared with the experimental results as shown in Figs. 5(a)-(f), which indicates that the calculated displacement of unconfined columns is slightly smaller than the measured one. This is mainly due to neglecting the slip between the steel bars and concrete in the numerical analysis. The larger stiffness difference between the numerical and experimental hysteretic loops shown in Fig. 5(a) could be induced by experimental errors.

The difference in the descending branch between the numerical and experimental results shown in Figs. 5(d)-(f) is due to the constitutive model of concrete adopted in OpenSees. As shown in Fig. 12(a), the constitutive model of CFRP confined concrete is approximated by projecting the stresses and strains at points A and B onto the unconfined concrete model. However, there exists a residual stiffness after point B in the Kent-Park model. In addition, the difference could be also induced by neglecting the slip between the steel bars and concrete.

As shown in Table 7, the calculated bearing capacity  $P_{num}$  is higher than the measured one  $P_{exp}$ , but the difference is smaller than 10%. Although there are slight differences between the calculated and measured hysteretic loops, the numerical results are still in good agreement with the experimental results.

### 3.4 Parametric study

A parametric study is conducted to analyze the seismic behaviors of partially deteriorated RC columns and the effect of confined CFRP sheets on the lateral bearing capacity. The key parameters include the length of the deteriorated concrete segment, the ratio of the CFRP thickness to the column diameter ratio  $t/D$ , the slenderness ratio of columns  $L/D$ , and the axial load ratio  $\lambda_{in}$ ,

where  $\lambda_{in}=P/(f_{in}A)$ . According to the parameters and the constitutive relationships of concrete and steel bars used in Section 3.2, the bearing capacities of 48 partially deteriorated columns were predicted. The bearing capacities of 48 partially deteriorated columns with CFRP thicknesses of 0 mm, 0.167 mm, 0.334 mm, and 0.501 mm, slenderness ratios of 4, 5, and 6, and axial load ratios of 0.1, 0.2, 0.3, and 0.4 are evaluated by the finite element method. The lateral bearing capacities of partially deteriorated columns were shown in Table 8. In Table 8, the specimen is denoted as “XXab”, where “XX” represents group, i.e., SL, TL, and ST, “a” the slenderness ratio, and “b” the axial load ratios of 1, 2, 3, and 4, corresponding to 0.1, 0.2, 0.3, and 0.4.

### 3.4.1 Effect of length of deteriorated concrete segment on seismic behaviors

Fig. 13 shows the hysteretic loops of partially deteriorated RC columns with different lengths of the deteriorated concrete segment.  $l_w$  is the ratio of the length of the deteriorated concrete segment to the height of the column. It can be seen from Fig. 13 that the displacements of partially deteriorated columns increase with the increase of the length of the deteriorated concrete segment, but the bearing capacities are basically the same. Therefore, the seismic behaviors of columns are seldom affected by the length of the deteriorated concrete segment.

Table 8 Predicted lateral bearing capacity of specimens

Thickness of CFRP (mm)	Lateral bearing capacity (kN)											
	Specimen											
	SL41	SL42	SL43	SL44	SL51	SL52	SL53	SL54	SL61	SL62	SL63	SL64
	(TL41)	(TL42)	(TL43)	(TL44)	(TL51)	(TL52)	(TL53)	(TL54)	(TL61)	(TL62)	(TL63)	(TS64)
(ST41)	(ST42)	(ST43)	(ST44)	(ST51)	(ST52)	(ST53)	(ST54)	(ST61)	(ST62)	(ST63)	(ST64)	
0	57.3	54.8	50.9	46.4	42.6	40.3	39.9	34.5	35.7	35.3	31.1	27.2
0.167	62.7	61.9	60.8	58.5	47.5	46.4	44.6	41.3	38.0	37.6	35.3	30.5
0.334	66.8	65.2	64.0	62.0	48.8	47.9	45.8	43.2	39.0	38.5	35.8	31.6
0.501	70.0	68.7	67.1	64.0	49.5	48.6	46.9	44.0	40.0	39.5	37.2	32.3

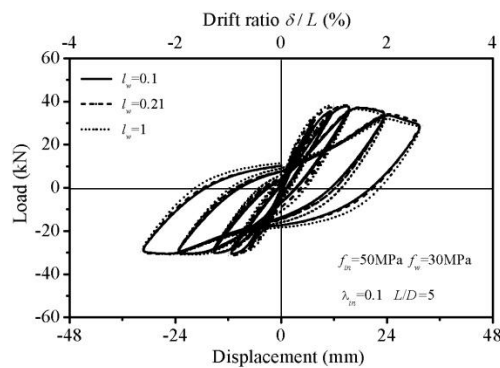


Fig. 13 Hysteretic loops of deteriorated columns with different lengths of deteriorated concrete

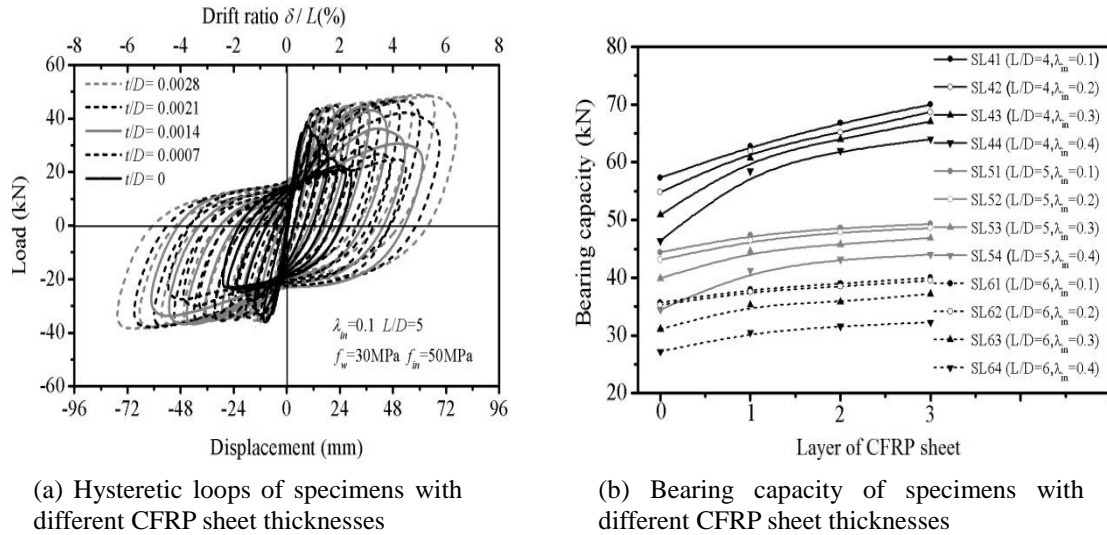


Fig. 14 Effect of CFRP sheet thickness on bearing capacity

### 3.4.2 Effect of CFRP confinement ratio on retrofitting effect

The hysteretic loops of partially deteriorated columns retrofitted with different CFRP thicknesses are shown in Fig. 14(a). The lateral bearing capacities for  $t/D$  at 0, 0.0007, 0.0014, 0.0021, and 0.0028 are 42.6 kN, 47.5 kN, 48.8 kN, 49.5 kN, and 49.8 kN, respectively. Thus, the lateral bearing capacities for  $t/D$  at 0.0007, 0.0014, 0.0021 and 0.0028 are larger than that for  $t/D$  at 0 by 11.5%, 14.5%, 16.1%, and 16.9%, respectively. Therefore, the ultimate bearing capacity and ultimate displacement increases with the increase of  $t/D$ , but the increment decreases gradually. Wrapping CFRP sheets with a  $t/D$  of 0.0021, i.e., three layers of CFRP sheets, is considered to be effective.

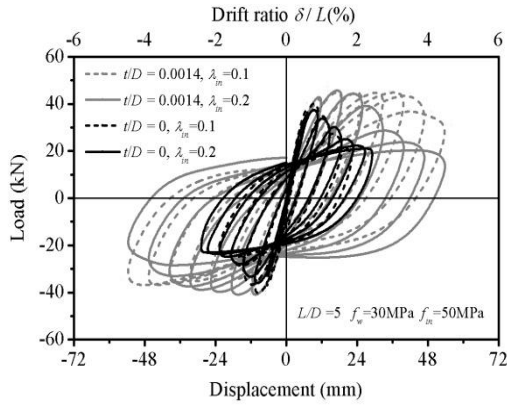
The bearing capacities of partially deteriorated columns are shown in Fig. 14(b). It can be seen from Fig. 14(b) that, as the number of CFRP layers increases, the bearing capacities of specimens with different axial load ratios and slenderness ratios increase to different extents. For each specimen, one layer of CFRP is the most efficient in improving the bearing capacity, especially for specimens with high axial load ratios and low slenderness ratios.

### 3.4.3 Effect of axial load ratio on retrofitting effect

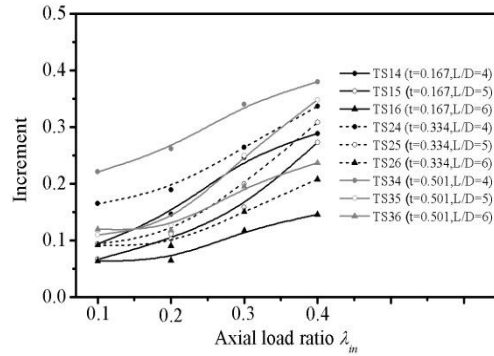
Figs. 15(a)-(b) show the hysteretic loops of partially deteriorated and retrofitted columns under different axial load ratios. As shown in Fig. 15(a), the effect of wrapping CFRP with the same thickness on the bearing capacities of partially deteriorated columns is different for different axial load ratios. When  $\lambda_{in}$  is 0.1, the lateral bearing capacity of CFRP retrofitted columns is 48.8 kN, larger than that of partially deteriorated columns by 14.5%. When  $\lambda_{in}$  is equal to 0.2, the lateral bearing capacity of CFRP retrofitted columns is 47.9 kN, larger than that of partially deteriorated columns by 19%. Fig. 15(b) shows the incremental lateral bearing capacities of specimens, which indicates that the bearing capacities of specimens increase by increasing the axial load ratio and that the contribution of each layer of CFRP also increases with an increase in the axial load ratio. The smaller the axial load ratio is, the smaller the effect of CFRP sheets on the bearing capacity is.

3.4.4 Effect of axial load ratio on retrofitting effect

Figs. 16(a)-(b) show the hysteretic loops of partially deteriorated and retrofitted columns with different slenderness ratios. As can be seen from Fig. 16(a), the lateral bearing capacities of unconfined partially deteriorated columns and retrofitted substandard columns with two layers of CFRP and a  $L/D$  of 4 are 57.3 kN and 66.8 kN, but the two values are equal to 42.6 kN and 48.8 kN for  $L/D = 5$ . For  $L/D=4$  and 5, wrapping two layers of CFRP increases the lateral bearing capacity by 16.5% and 14%, respectively. The effect of CFRP sheets on the lateral bearing capacity of deteriorated columns are shown in Fig. 16(b). It can be seen from Fig. 16(b) that, most of the curves are concave and the incremental lateral bearing capacity decreases with the increase of the slenderness ratio.

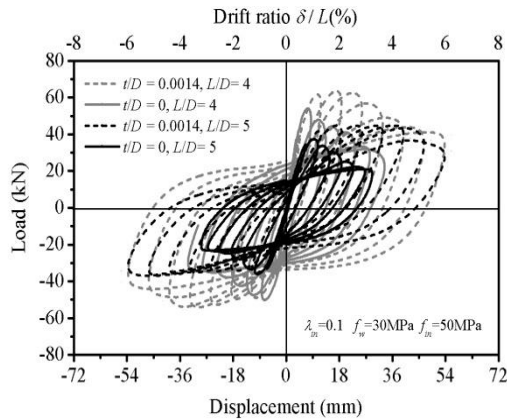


(a) Hysteretic loops of specimens with different axial loads

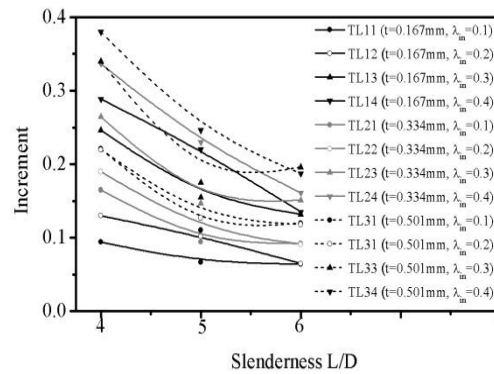


(b) Bearing capacity of specimens with different axial loads

Fig. 15 Effect of axial load ratio on bearing capacity



(a) Hysteretic loops of specimens with different slenderness ratios



(b) Bearing capacity of specimens with different slenderness ratios

Fig. 16 Effect of slenderness ratio on bearing capacity

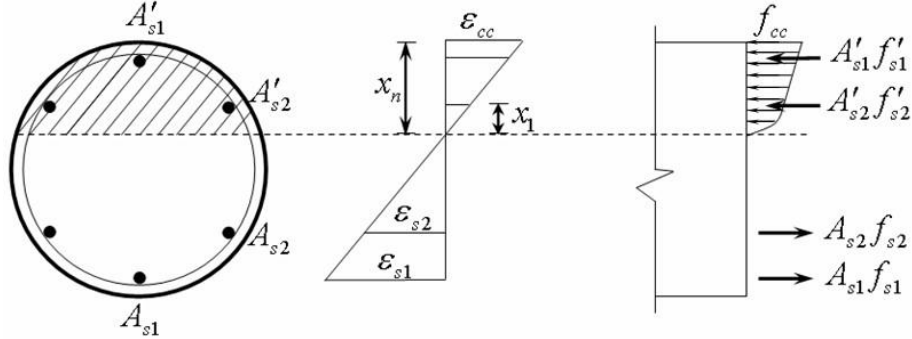


Fig. 17 Stress and strain distributions on circular cross section

## 4. Determination of CFRP thickness

### 4.1 Basic assumptions

In the following analysis, assumptions are made as follows:

- (1) The cross section remains plane after bending.
- (2) The confinement of stirrups and shear deformation are neglected.
- (3) The interfaces between the steel bars, FRP sheets, and concrete are perfect.
- (4) The Teng *et al.* model, Teng *et al.* (2009) and Lam *et al.* (2003), is adopted for CFRP confined concrete.
- (5) Steel bars are considered to be an elastic-perfectly plastic material (Yuan *et al.* 2008).

### 4.2 Ultimate bearing capacity of CFRP retrofitted substandard columns

According to the basic assumptions, the stress and strain distributions are shown in Fig. 17, where  $R$  is the radius of the circular section,  $A_{si}'$  and  $f_{si}$ ,  $A_{si}$  and  $f_{si}$  are the areas and stresses of the  $i^{\text{th}}$  row steel bars in the compression and tension zones, respectively, and  $x$  is the distance from the neutral axis. The axial force  $N$  and bending moment  $M_w$  are determined from the equilibrium of forces as follows

$$N = 2 \int_0^{x_1} \left[ E_c \frac{x}{x_n} \varepsilon_{cc} - \frac{(E_c - E_2)^2}{4f_{c0}} \left( \frac{x}{x_n} \varepsilon_{cc} \right)^2 \right] \sqrt{R^2 - (x + R - x_n)^2} dx + 2 \int_{x_1}^{x_n} \left[ f_{c0} + E_2 \frac{x}{x_n} \varepsilon_{cc} \right] \sqrt{R^2 - (x + R - x_n)^2} dx + \sum_{i=1}^n f_{si} A_{si} \quad (1)$$

$$M_w = 2 \int_0^{x_1} \left[ E_c \frac{x}{x_n} \varepsilon_{cc} - \frac{(E_c - E_2)^2}{4f_{c0}} \left( \frac{x}{x_n} \varepsilon_{cc} \right)^2 \right] \sqrt{R^2 - (x + R - x_n)^2} x dx + 2 \int_{x_1}^{x_n} \left[ f_{c0} + E_2 \frac{x}{x_n} \varepsilon_{cc} \right] \sqrt{R^2 - (x + R - x_n)^2} x dx + \sum_{i=1}^n f_{si} A_{si} x_i + P(R - x_n) \quad (2)$$

where  $f_{c0}$  and  $f_{cc}$  are the strengths of unconfined and CFRP confined concrete,  $E_c$  is the elastic modulus of unconfined concrete,  $E_2$  is the slope of the linear portion in the stress-strain relationship of CFRP confined concrete,  $x_i$  is the distance from the  $i^{\text{th}}$  row bars to the neutral axis,  $\varepsilon_{si}$  is the strain in the  $i^{\text{th}}$  row bars,  $\varepsilon_{cc}$  is the ultimate strain of CFRP confined concrete,  $x_1$  is the distance from the intersection point of the confined concrete model to the neutral axis,  $x_n$  is the distance from the edge of the compression zone to the neutral axis.

### 4.3 Ultimate lateral bearing capacity of intact RC columns

The ultimate bearing capacity of intact RC columns is given by (GB50010-2010 (2010))

$$N = \alpha f_{c0} A \left( 1 - \frac{\sin(2\pi\alpha)}{2\pi\alpha} \right) + (\alpha - \alpha_t) f_y A_s \quad (3)$$

$$M_{in} = f_{c0} A R \frac{2\sin^3(\pi\alpha)}{3\pi} + f_y A_s r_s \frac{\sin(\pi\alpha) + \sin(\pi\alpha_t)}{\pi} \quad (4)$$

where  $\alpha$  is the central angle of the neutral axis,  $\alpha_t$  is between 1.25 and  $2\alpha$ ,  $r_s$  is the distance from the center of longitudinal bars to that of the circular section,  $M_{in}$  is the bending moment. When  $M_w$  is larger than  $M_{in}$ , CFRP sheets are required and the thickness can be determined from Eqs. (1)-(4). The bearing capacity  $P_{sec}$  of the control column, partially deteriorated columns, and the retrofitted columns are evaluated as shown in Table 7, which indicates that the proposed method can predict the bearing capacity of retrofitted deteriorated columns with reasonable accuracy.

### Acknowledgments

The financial support from the National Natural Science Foundation with Grant Nos. 50578025 and 51421064 and the National Basic Research Program (973 Program) with Grant No. 2009CB623200, of the People's Republic of China, is greatly acknowledged.

### References

- Akgun, D., Demir, C. and Ilki, A. (2010), "Axial behavior of FRP jacketed extended rectangular members constructed with low strength concrete", *The 5th International Conference on FRP Composites in Civil Engineering*, Beijing, China, September.
- Bailey, C. and Yaqub, M. (2012), "Seismic strengthening of shear critical post-heated circular concrete columns wrapped with FRP composite jackets", *Compos. Struct.*, **94**(3), 851-864.
- Bao, X. and Li, B. (2010), "Residual strength of blast damaged reinforced concrete columns", *Int. J. Impact Eng.*, **37**(3), 295-308.
- Belarbi, A. and Bae, S. (2007), "An experimental study on the effect of environmental exposures and corrosion on RC columns with FRP composite jackets", *Compos. Part B-Eng.*, **38B**(5-6), 674-684.
- CEB-FIP (2010), *CEB-FIP*, CEB-FIP Model Code, Lausanne.
- EIGawady, M., Endeshaw, M., McLean, D. and Sack, R. (2010), "Retrofitting of rectangular columns with deficient lap splices", *J. Compos. Constr.*, **14**(1), 22-35.
- Emmanuel, A. and Oladipo, F. (2012), "Investigation of salinity effect on compressive strength of reinforced concrete", *J. Sustain. Dev.*, **5**(6), 74-82.
- Frangou, M., Pilakoutas, K. and Dritsos, S. (1995), "Structural repair/strengthening of RC columns", *Constru. Build. Mater.*, **9**(5), 259-266.
- Fukuyama, K., Higashibata, Y. and Miyauchi, Y. (2000), "Studies on repair and strengthening methods of damaged reinforced concrete columns", *Cement. Concrete. Comp.*, **22**(1), 81-88.
- GB50010-2010 (2010), *GB50010-2010*, Code for design of concrete structures, Beijing.
- Goksu, C., Polat, A. and Ilki, A. (2012), "Attempt for seismic retrofit of existing substandard RC members under reversed cyclic flexural effects", *J. Compos. Constr.*, **16**(3), 286-299.
- Hanjari, K. (2010), "Structural behaviour of deteriorated concrete structures", Ph.D. Dissertation, Chalmers University of Technology, Göteborgs.
- Harajli, M. (2008), "Seismic behavior of RC columns with bond-critical regions: criteria for bond

- strengthening using external FRP jackets”, *J. Compos. Constr.*, **12**(1), 69-79.
- Haroun, M. and Elsanadedy, H. (2005), “Fiber-reinforced plastic jackets for ductility enhancement of reinforced concrete bridge columns with poor lap-splice detailing”, *J. Bridge. Eng.*, **10**(6), 749-757.
- Iacobucci, R., Sheikh, S. and Bayrak, O. (2003), “Retrofit of square concrete columns with carbon fiber-reinforced polymer for seismic resistance”, *ACI Struct. J.*, **100**(6), 785-794.
- Kalyoncuoglu, A., Ghaffari, P., Goksu, C. and Ilki, A. (2013), "Rehabilitation of corrosion-damaged substandard RC columns using FRP sheets”, *Adv.Mat.Res.*, **639-640**, 1096-1103.
- Kent, D. and Park, R. (1971), “Flexural members with confined concrete”, *J. Struct. Div.*, **97**(7), 1969-1990.
- Lam, L., and Teng, J. (2003), “Design-oriented stress–strain model for FRP-confined concrete”, *Constr. Build. Mater.*, **17**(6), 471-489.
- Li, B. and Lim, C. (2010), “Tests on seismically damaged reinforced concrete structural walls repaired using fiber-reinforced polymers”, *J. Compos. Constr.*, **14**(5), 597-608.
- Li, G., Hedlund, S., Pang, S., Alaywan, W., Eggers, J. and Abadie, C. (2003), “Repair of damaged RC columns using fast curing FRP composites”, *Compos. Part B-Eng.*, **34B**(3), 261-271.
- Li, J., Gong, J. and Wang, L. (2009), “Seismic behavior of corrosion-damaged reinforced concrete columns strengthened using combined carbon fiber-reinforced polymer and steel jacket”, *Constr. Build. Mater.*, **23**(7), 2653-2663.
- Manuel, A. and Silva (2011), “Behavior of square and circular columns strengthened with aramidic or carbon fibers”, *Constr. Build. Mater.*, **25**(8), 3222-3228.
- Mazzoni, S., McKenna, F. and Scott, H. (2009), *Open System For Earthquake Engineering Simulation User Command-language Manual*, Pacific earthquake engineering research center, Berkeley, California, USA.
- Ozcan, O., Binici, B. and Ozcebe, G. (2008), “Improving seismic performance of deficient reinforced concrete columns using carbon fiber-reinforced polymers”, *Eng. Struct.*, **30**(6), 1632-1646.
- Ozcan, O., Binici, B. and Ozcebe, G. (2010), “Seismic strengthening of rectangular reinforced concrete columns using fiber reinforced polymers”, *Eng.Struct.*, **32**(4), 964-973.
- Pantazopoulou, S. J., Bonacci, J., Sheikh, S., Thomas, M. and Hearn, N. (2001), “Repair of corrosion-damaged columns with FRP wraps”, *J. Compos. Constr.*, **5**(1), 3-11.
- Pantelides, C., Gergely, J., Reaveley, L. and Volnyy, V. (1999), “Retrofit of RC bridge pier with CFRP Advanced Composites”, *J. Struct. Eng.*, **125**(10), 1094-1099.
- Rousakis, T. and Karabinis, A. (2008), “Substandard reinforced concrete members subjected to compression: FRP confining effects”, *Mater. Struct.*, **41**(9), 1595-1611.
- Saadatmanesh, H., Ehsani, M.R. and Jin, L. (1997a), “Repair of earthquake-damaged RC columns with FRP wraps”, *ACI Struct. J.*, **94**(2), 206-215.
- Saadatmanesh, H., Ehsani, M.R. and Jin, L. (1997b), “Seismic retrofitting of rectangular bridge columns with composite straps”, *Earthq. Spectra.*, **13**(2), 281-304.
- Saadatmanesh, H., Ehsani, M.R. and Li, M.W. (1994), “Strength and Ductility of concrete columns Externally Reinforced with Fiber Composite Strapes”, *ACI Struct. J.*, **91**(4), 434-447.
- Saadatmanesh, H., Ehsani, M.R. and Jin, L. (1996), “Seismic strengthening of circular bridge pier model with fiber composites”, *ACI Struct. J.*, **93**(6), 639-647.
- Seible, F., Priestley, M.J.N., Hegemier, G.A. and Innamorato, D. (1997), “Seismic retrofit of RC columns with continuous carbon fiber jackets”, *J. Compos. Constr.*, **1**(2), 52-62.
- Sheikh, S.A. and Bayrak, O. (2001), “Seismic behaviour of FRP-Retrofitted concrete columns”, *Proceedings of Structures Congress 2001*, Washington D.C., USA, May.
- Sheikh, S.A. and Yau, G. (2002), “Seismic behavior of concrete columns confined with steel and fiber-reinforced polymers”, *ACI Struct. J.*, **99**(1), 72-80.
- Scott, B.D, Park, R. and Priestley, M.J.N (1982), “Stress-strain behavior of concrete confined by overlapping hoops at low and high strain rates”, *ACI Mater. J.*, **79** (1), 13-27.
- Teng, J., Jiang, T., Lam, L. and Luo, Y. (2009), “Refinement of a design-oriented stress--strain model for FRP-confined concrete”, *J. Compos. Constr.*, **13**(4), 269-278.
- Thermou, G.E. and Pantazopoulou, S.J. (2009), “Fiber-reinforced polymer retrofitting of predamaged substandard RC prismatic members”, *J. Compos. Constr.*, **13**(6), 535-546.

- Wei, H., Wu, Z. and Zhang, P. (2010), "Axial experiment on CFRP confined steel reinforced concrete columns with partial deteriorated strength", *J. Reinf. Plast. Comp.*, **29**(6), 874-882.
- Wei, H., Wu, Z., Guo, X. and Yi, F. (2009), "Experimental study on partial deteriorated strength concrete columns confined with CFRP", *Eng. Struct.*, **31**(10), 2495-2505.
- Wei, H. (2009), "Compressive performance study on CFRP wrapped concrete columns with partial deteriorated strength", Ph.D. Dissertation, Dalian University of technology, Dalian.
- Xiao, Y., Wu, H. and Martin, G.R. (1999), "Prefabricated composite jacketing of RC columns for enhanced shear strength", *J. Struct. Eng.*, **125**(3), 255-264.
- Yalcin, C. and Kaya, O. (2004), "An experimental study on the behavior of reinforced concrete columns using FRP material", *13th World Conference on Earthquake Engineering*, Vancouver B.C., Canada, August.
- Yalcin, C., Kaya, O. and Sinangil, M. (2008), "Seismic retrofitting of R/C columns having plain rebars using CFRP sheets for improved strength and ductility", *Constr. Build. Mater.*, **22**(3), 295-307.
- Yu, J., Zhang, Y. and Lu, Z. (2014), "Seismic rehabilitation of RC frame using epoxy injection technique tested on shaking table", *Struct. Eng. Mech.* **52**(3), 541-558.
- Yuan, X., Xia, S., Lam, L. and Smith, S.T. (2008), "Analysis and behaviour of FRP-confined short concrete columns subjected to eccentric loading", *J. Zhejiang. Univ- Sc A.*, **1**(9), 38-49.
- Zhu, Z., Ahmad, I. and Mirmiran, A. (2006), "Fiber element modeling for seismic performance of bridge columns made of concrete-filled FRP tubes", *Eng. Struct.* **28**(14), 2023-2035.